Desalination and Water Treatment
www.deswater.com
doi: 10.5004/dwt.2022.28119

249 (2022) 23–32
February

Bioinspired fabrication of composite ultrafiltration membrane with high performance for wastewater treatment

Guocheng Song[a,*], Chun Ding[b]

[a]*College of Materials Science and Engineering, Jiujiang University, 551 East Qianjin Road, Lianxi District, Jiujiang City, Jiangxi Province, China, Tel. +86-186-1512-7724; email: sgc_34@163.com*
[b]*College of Economics, Jiujiang University, 551 East Qianjin Road, Lianxi District, Jiujiang City, Jiangxi Province, China, Tel. +86-136-4644-5811; email: 478811074@qq.com*

Received 21 August 2021; Accepted 1 January 2022

ABSTRACT

In this paper, we prepared a novel kind of composite ultrafiltration (UF) membrane with high flux, super-hydrophilicity and self-cleaning properties via vacuum filtration technique. The nitrocellulose porous membrane was selected as the substrate while an ultrathin and integral sodium alginate (SA) layer was first formed on its surface with crosslinking treatment via vacuum filtration at 0.05 MPa, then the polydopamine (PDA) was deposited on the surface of the SA layer and the β-FeOOH nanorods were immobilized on PDA layer through bio-mineralization process. The composite membranes were applied in filtration tests of protein solutions (BSA and Lyz) and oil in water emulsions separation. The results showed that membranes with PDA and β-FeOOH nanorods modified exhibited a high operational flux and excellent antifouling property due to the superhydrophilicity and surface nanoscale hierarchical structures. Moreover, the mineralized composite membrane exhibited satisfactory stability during the recycling filtration process, suggesting great potential for the long-term application. The dye wastewater was efficiently degraded by β-FeOOH layer through Fenton reaction in the presence of visible light and hydrogen peroxide, which additional endowing the modified membranes with effective filtration performance and self-cleaning capability. In conclusion, this work offered a convenient and facile way to construct UF membrane with high separation efficiency and remarkable antifouling ability which had great potential in wastewater treatment.

Keywords: Vacuum filtration; β-FeOOH nanorods; Composite; Mineralization; Antifouling

1. Introduction

With the development of technology and industrialization, while bringing benefits and convenience to human lives, the global water pollution problems also menace the public health and lead to severe challenges such as ecosystem deterioration or global disease [1,2]. Compared with traditional technologies containing absorption, coagulation, water evaporation, biodegradation and de-emulsification, membrane-based technologies have drawn considerable research attentions to purifying and reusing industrial wastewater due to the advantages of wide application range, simple separation equipment, high separation efficiency, low energy consumption and easy operation [3–6]. Ultrafiltration (UF) membrane as one kind of various separation membranes has been widely used in the field of water purification and recycling, such as wastewater treatment, food industry, pharmaceuticals and bio-engineering [7–11]. The conventional ways of UF membranes are usually carried out by phase inversion techniques with asymmetric

* Corresponding author.

porous structures [12]. Recent years, the UF membranes which contain porous substrates and ultrathin barrier layers can effectively conquer the above disadvantages, own high permeability and low energy cost in wastewater treatment applications [13–15]. These composite membranes are usually prepared via interfacial polymerization or surface coating technology [16–18], such as electrostatic powder coating or solution-blown spraying, but the barrier layers sometimes have the problem of inhomogeneous, incompact and poor adhesion for substrates. Vacuum filtration technology is a remarkably facile and convenient approach to prepare these composite membranes [19,20]. Jiang et al. [21] fabricated Janus membranes with hydrophilic polyacrylonitrile nanofiber membranes as substrate and single-side hydrophobic carbon nanotube as ultrathin barrier layer via vacuum filtration. The Janus membrane showed both satisfactory mechanical and chemistry stability, and had a switchable oil/water separation performance in different operating modes due to the asymmetric wettability on each side. In the oil/water separation test, it had an ultrahigh operational flux and separation efficiency owing to its highly porous and surface anisotropic nature. Xu et al. [22] prepared hierarchical filtration membranes by vacuum filtration of TiO_2 suspension with Graphene oxide-TiO_2 (GOT) composite sheets as substrate. The filtration properties of the composite films were evaluated by filtrating dye solution (Direct Red and Blue). The results indicated that the membranes possessed photocatalytic antifouling ability under concurrent UV light irradiation, which could effectively reduce the impacts of organic contaminants and obviously enhance their water treatment ability. Zhang et al. [23] prepared a novel membrane (FeTi–NWM) made of interwoven iron oxide (Fe_2O_3) nanowires and TiO_2 nanowires by a vacuum filtration and hot pressing method. The results showed under simulated solar irradiation the FeTi-NWM owned excellent anti-fouling capability which humic acid (HA) could be nearly completely removed during a 2 h short-term test. The mainly reasons could be attributed to the enhanced HA absorption by Fe_2O_3 nanowires and the formed Fe_2O_3/TiO_2 heterojunctions that increase photo-induced charge transfer and improve visible light activity.

The problem of membranes fouling is one of the main drawbacks which will reduce the separation efficiency, shorten membranes service lifespan, greatly increase the operating cost and limit their large-scale application [24,25]. To our knowledge, hydrophilic modification has been considered as a facile and effective method to improve antifouling performance of the membranes [26,27]. Zarghami et al. [28] fabricated an novel organic-inorganic hybrid recoverable membranes with high hydrophilicity and underwater oleophobicity via bio-inspired technique. The polydopamine (PDA) was immobilized on the surface of PES membranes while the amino-functionalized multi-wall carbon nanotubes (N-MWCNTs) were subsequently anchored onto the PDA layer. The water flux of newly developed PES/PDA/N-MWCNTs membranes significantly increased (~1,086%) compared to the unmodified PES membrane. The total fouling ratio (Rt) of the PES/PDA/N-MWCNTs membrane was 22.35% comparing with 98.38% of the unmodified PES membrane. Generally speaking, the combination of superhydrophilic and photo-induced self-cleaning ability can simultaneously construct a dense hydration layer to repel pollutants adsorption and degradate organic dyes under visible or UV light irradiation [29,30]. Zhao et al. [31] prepared CNT nanohybrid membranes embedded with FeOOH nanorods (NRs) which owned superhydrophilicity and photo-induced self-cleaning capability. The nanohybrid membrane possessed a high water permeability above 8,000 $Lm^2/h/bar$ and greatly elevated flux recovery ratio above 97% for oil/water separation. Lv et al. [32] fabricated a photocatalytic nanofiltration membrane (NFM) with self-cleaning property via a co-deposition method followed by mineralization of a photocatalytic layer consisting of β-FeOOH nanorods. In visible light, the β-FeOOH layer exhibited efficient photocatalytic activity for degrading dyes, endowing the NFM with effective antifouling performance and self-cleaning capability.

Drawing inspiration from vacuum filtration and bio-mineralization methodology, herein the composite UF membranes were fabricated by the use of the nitrocellulose (NC) microfiltration membrane as porous substrate and the sodium alginate (SA) as ultrathin hydrophilic barrier layer, the resulting SA barrier layer was prepared via vacuum filtration following by chemical crosslinking treatment. The polydopamine (PDA) was subsequently deposited on the surface of SA layer and then the β-FeOOH nanorods layer was generated on the surface of the PDA layer through a mineralization process to build nanoscale hierarchical structure. The composite membranes were applied in filtration separation of protein solutions (BSA and Lyz) and oil in water emulsions to observe the separation and antifouling abilities. The tests of dye degradation under visible light irradiation in the presence of hydrogen peroxide (H_2O_2) were also carried out to evaluate the membranes self-cleaning characteristics.

2. Experimental

2.1. Materials

BSA (pI = 4.8, 67 kDa), lysozyme (Lyz, pI = 10.8, 14.4 kDa), tris(hydroxymethyl) aminomethane (Tris), potassium dihydrogen phosphate (KH_2PO_4), dipotassium hydrogen phosphate trihydrate ($K_2HPO_4{\cdot}3H_2O$), iron chloride hexahydrate ($FeCl_3{\cdot}6H_2O$), H_2O_2 (30% in H_2O), calcium chloride anhydrous ($CaCl_2$), sodium alginate (SA), Methylene blue and silicone oil were obtained from Sinopharm Chemical Reagent Co., Ltd., (Shanghai, China) and used without further purification. Tween 80 was acquired from Ling Feng Chemicals Co., Ltd., (Shanghai, China). DA hydrochloride (99%) was purchased from Shanghai Titan Scientific Co., Ltd (Shanghai, China). The nitrocellulose (NC, mean pore size was 0.45 μm) microfiltration membranes were purchased from Haining Yibo filter equipment Co., Ltd., (Haining, China).

2.2. Fabrication of the nitrocellulose/sodium alginate (NC-SA) membrane

The NC membranes were washed in deionized water/ethanol (v/v = 1/1) for 2 h and then soaked in ultrapure water for 24 h to remove the ethanol. The sodium alginate (SA) power was added into deionized water using mechanical stirring at 65°C until the powder fully dissolved to form

uniform mixed solution with the concentration of 0.5 wt.%. The SA suspension was permeated through a glass filter which the NC membrane was placed in it by vacuum filtration at 0.05 MPa. Different amount of SA was deposited on the NC membranes surface to form a uniform ultrathin barrier layer. The theoretical depositing degree (TDD) was about 2.0, 4.0 and 6.0 mg/cm^2 respectively, which the corresponding modified membranes were labelled as NC-SA2, NC-SA4, NC-SA6 membranes respectively. The above composite membranes were dried under vacuum at 60°C for 2 h and then followed by the crosslinking treatment in 50 mL $CaCl_2$ solution with the concentration of 4 wt.% for 15 min at room temperature. Thereafter, the composite membranes were cleaned in deionized water/ethanol (v/v = 1/1) for 60 min and then washed with deionized water for 48 h to remove non-firmly deposited SA power. Then they were dried under vacuum at 60°C for 12 h to a constant weight. The actual depositing degree (ADD) was calculated as the following equation:

$$\mathrm{ADD} = \frac{W_1 - W_0}{A} \tag{1}$$

where W_0 was the weight (mg) of the initial NC membrane, W_1 was the weight (mg) of the NC-SA membrane, A represented the area of the membrane (cm^2).

2.3. Fabrication of the nitrocellulose/sodium alginate/polydopamine (NC-PDA) membrane

1 g/L dopamine solution was prepared in Tris buffer (pH 8.5, 10 mM) solution using mechanical stirring to form uniform solution. Then the NC-SA4 membranes were slightly placed on the surface of the mixed solution which the SA side faced down under static condition at room temperature (~30°C) for 8 h. The composite membrane with PDA coating was taken out and washed with ultrapure water and ethanol alternately by gentle shaking for 24 h to remove the free PDA particles, and then dried in a vacuum oven at 60°C for 12 h. The resultant membrane was referred as NC-PDA membrane.

2.4. Fabrication of the nitrocellulose/sodium alginate/polydopamine/β-FeOOH (NC-FeOOH) membrane

A certain amount of $FeCl_3{\cdot}6H_2O$ was fully dissolved in 20 ml deionized water with the concentration of 18 mg/ml, and then 10 mL hydrochloric acid (10 mmol/L) was added to prepare the mineralizing solution. The NC-PDA membranes were immersed in this solution for 24 h at 60°C to induce the β-FeOOH nanorods generation. Finally, the mineralized modified membranes were washed with deionized water for 24 h to eliminate the loose stacking β-FeOOH nanorods and dried in a vacuum oven at 60°C for 12 h. The obtianed mambrane was named as NC-FeOOH membrane.

2.5. Separation experiment of protein solutions

In order to further evaluate the filtration and antifouling properties of the modified membranes, a dead-end filtration system which contained air pump, flow meter, and filtering vessel was prepared by ourselves in laboratory. The effective membranes area was about 10 cm^2. The composite membranes were placed into the filtration cell which the modified sides faced the feed solution. Before the filtration test, the membranes were carried out for 30 min by filtering pure water at 0.15 MPa. Then the pressure was adjusted to 0.10 MPa and the volume of permeated water was measured every 5 min for five times to obtain an average value. The pure water flux (J_w) was calculated by the following equation:

$$J_w = \frac{V}{A \times t} \tag{2}$$

where V was the volume of the permeated water during the filtration time (L), A was the effective membrane area (m^2), t was the filtration time (h).

After the pure water filtration, the proteins (BSA and Lyz) were respectivly added into phosphate buffer solution (PBS, pH = 7.0, 10 mM) under mechanical agitation to prepare filtration suspension with concentration of 1.0 g/L. Each filtration recycling process of protein solutions were measured for 2 h at 0.1 MPa, and the permeation flux was calculated every 5 min to observe the variable regularity.

While each round of filtration test was finished, the composite membranes were only simply washed with tap water for about 30 min, and the recovery pure water flux (J_p) was measured again at 0.1 MPa. The fouling resistance of the membranes was evaluated by flux recovery ratio (FRR%) using the following equation:

$$\mathrm{FRR}(\%) = \frac{J_p}{J_w} \times 100\% \tag{3}$$

The protein rejection (R%) was calculated by the following equation:

$$R(\%) = \left(1 - \frac{C_p}{C_f}\right) \times 100\% \tag{4}$$

where C_p and C_f were the concentration of protein in the permeate and feed solution, respectively.

The above filtration separation cycle was repeated three times and at least three samples of each film were chosen to carry out the filtration experiments to acquire the mean value.

2.6. Separation experiment of oil in water emulsions

The preparation of oil in water emulsions could refer to our previous work [33]. The recovery pure water permeate flux was calculated using Eq. (2), the oil rejection (Roil%) was calculated by Eq. (3), and the flux recovery ratio (FRR%) was evaluated by Eq. (4). The operation of oil in water emulsions separation were similar to the filtration of proteins solution and repeated three times to evaluate the durability of the membranes. Each result is an average of at least three parallel experiments.

2.7. Evaluation of the static self-cleaning performance

The static self-cleaning performance of the NC-FeOOH membrane was evaluated by photocatalytic degradation of Methylene blue. Methylene blue (50 mL, 10 mg/L, pH = 3.0) and H_2O_2 (30%, 5 μL) were added into the container and settled under visible light which generated by an Xe lamp (500 W) equipped with a cutoff filter of 420 nm. A NC-FeOOH membrane was immersed in the dyes solution and the photocatalytic degradation time was 4 h and 8 h respectively at room temperature for photocatalysis. A cooling water bath was placed between the light source and the transparent container in case the overtemperature of the solution. The static photocatalytic operations were simply observed to evaluate the photocatalytic property of the membranes.

2.8. Characterization

The morphology and composition of the membranes were observed using a field-emission scanning electron microscopy (FESEM, Hitachi S-4800, Japan) and energy-dispersive X-ray spectroscopy (EDS, Hitachi S-4800, Japan). The modified side of samples were dried under vacuum at 60°C for 24 h and were coated with gold prior to detect the surface morphology.

The modified side of samples were evaluated by Attenuated total reflectance-Fourier-transform infrared spectroscopy (ATR-FTIR, Nicolet Nexus 8700 spectroscope, Thermo Fisher Scientific, USA) with the range of 4000–600 cm^{-1} to characterize the chemical structure and characterization of the membranes.

The static water contact angle (WCA) measurements for the modified side of samples were performed using a contact angle goniometer Kino SL200B by the sessile drop method at room temperature. The images were recorded immediately (~3 s) and the mean WCA results were obtained by measuring at least 10 contact angles to evaluate a mean value.

The crystalline structure of the composite membranes were measured by X-ray diffraction (XRD) which was performed on a D8 Advance X-ray diffractometer (Bruker, Germany) with 2θ between 10° and 60°.

The roughness parameters (Ra) of samples were measured by a non-contact optical profilometry using an interferometer profiler (Wyko-Veeco, model NT9100, USA), and the mean Ra results were calculated by measuring at least 3 spots of each membrane to obtain.

The proteins and oil concentrations of both feed and permeate solutions and the UV-Vis absorbance of Methylene blue before and after illumination were measured using a UV-9100 spectrophotometer (LabTech, Beijing).

3. Results and discussion

3.1. Morphology of the membranes

The surface morphology of the membranes were observed by scanning electron microscopy (SEM) in Fig. 1a–e. It could be seen that the original NC membrane was porous structure. When the TDD was about 2.0 mg/cm^2, the SA could not cover the surface of the NC membrane completely (Fig. 1b). Dramatic changes of the membranes morphology occurred along with the increase of SA deposition, an ultrathin integrated SA barrier was formed while the TDD was about 4.0 mg/cm^2. The actual depositing degree (ADD) of NC-SA2, NC-SA4 and NC-SA6 membranes were about 1.3, 2.8 and 4.2 mg/cm^2 respectively due to leaching out of SA with poor adhesion force. The surface color of the modified sides changed from white to light yellow after SA coating. The membranes surface morphology was very similiar between 4.0 and 6.0 mg/cm^2 of TDD except for different thickness of SA layer. Thus the SEM image of NC-SA6 is not described in Fig. 1. Then the PDA was adhered to the SA side of NC-SA4 membrane, and appearance of PDA side gradually changed into dark brown. The PDA particles sometimes could agglomerate into nanospheres maybe due to they were easy to accumulate under the condition of oxygen (Fig. 1d) [34]. Finally through *in suit* mineralization process, the PDA surface was uniformly decorated with β-FeOOH nanorods which could be observed in Fig. 1e. The EDS elemental map revealed that Fe element existed on the surface of the membrane which proved the successful mineralization. The surface appearance changed from dark brown to reddish brown mainly due to the existence of β-FeOOH nanorods on the PDA layer. This nanoscale hierarchical structures were beneficial for membrane permeability and preventing the pollutants adsorption [35].

3.2. Composition analysis of the membranes

The surface structure of the membranes was investigated by the ATR-FTIR spectra and is shown in Fig. 2. The absorbance at 1,650 cm^{-1} corresponded to the stretching vibration of N=O on the NC membranes, the characteristic adsorption of the C–O vibration was present at 1,277 cm^{-1}. The peak at about 1,060 cm^{-1} suggested the stretching vibration of C–N bond. The peak at about 832 cm^{-1} suggested the stretching vibration of C–O–C stretching vibration. The broad peak around 3,350 cm^{-1} were associated with the vibration of –OH group which would be favorable for the hydrophilic of membranes. When the integrated SA barrier layer was formed on the surface of CA membrane, except for the asymmetric stretching vibration of COO^- in 1,532 cm^{-1} and the increasing absorption peak intensity around 3,300 cm^{-1}, there was no obvious difference comparing with CA membrane which maybe due to the coincidence of the N=O and C–N vibration. When the PDA was deposited on the surface of SA layer, no significant changes in the spectra were detected, only the intensity of some absorption peaks had slightly changed such as 1,532 and 2,920 cm^{-1}. The reason was mainly due to the PDA layer was too thin to detect. After mineralization, the β-FeOOH nanorods were immobilized on the surface of PDA, the absorption peak in 1,410 cm^{-1} was the bending vibration of –OH, the peak in 690 cm^{-1} suggested the stretching vibration of Fe–O, and the intensity of the peaks in 1,600, 1,280 and 832 cm^{-1} decreased obviously owing to the coverage of β-FeOOH layer which illustrated that the β-FeOOH nanorods were successful deposited on the surface of membrane.

The crystal structures of the membranes were characterized by XRD and are shown in Fig. 3. The NC membrane, NC-SA membrane and NC-PDA membrane were almost

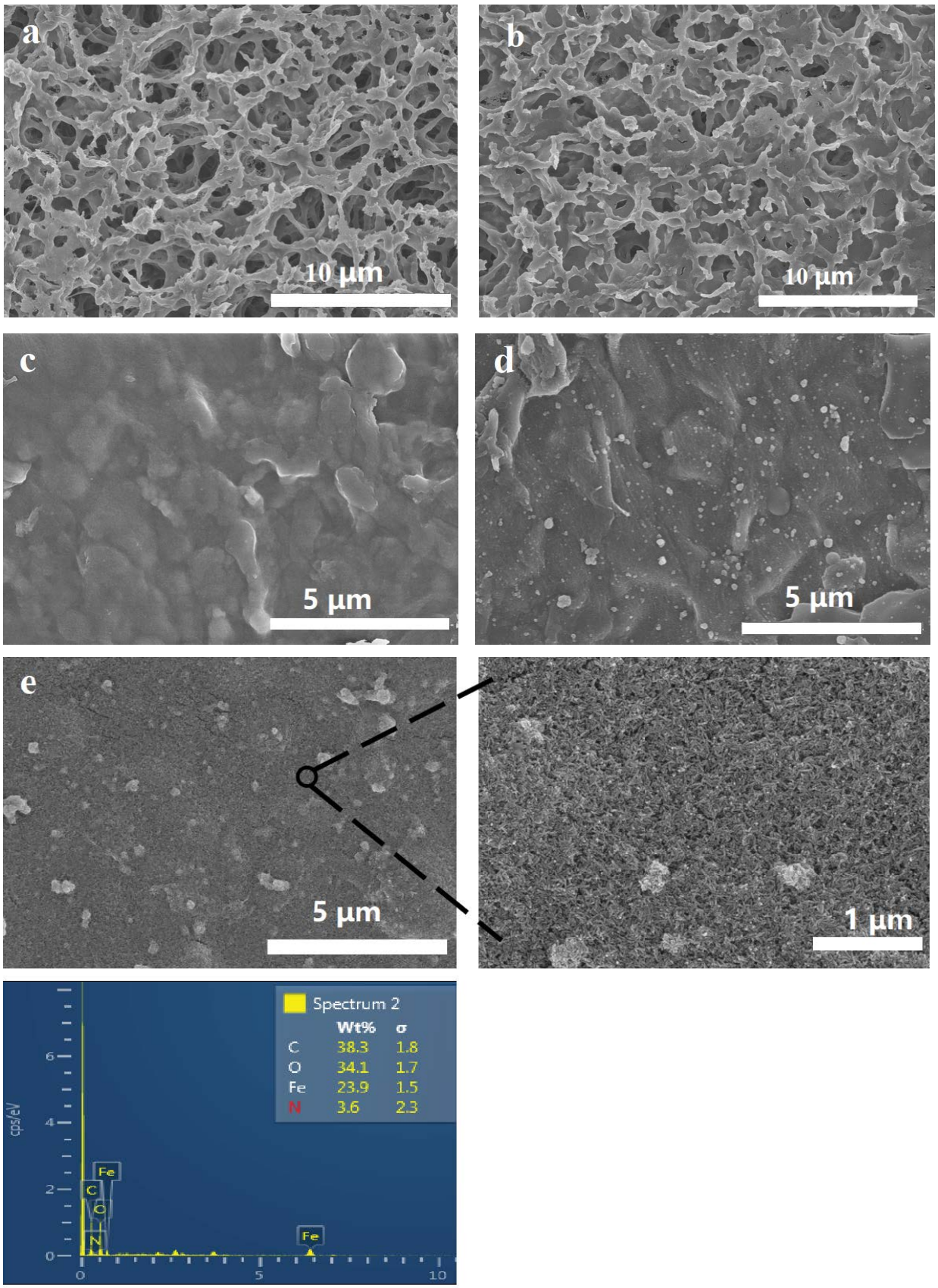

Fig. 1. SEM images of the membranes, (a) NC membrane, (b) NC-SA2 membrane, (c) NC-SA4 membrane, (d) NC-PDA membrane, (e) SEM image and EDS map of NC-FeOOH membrane.

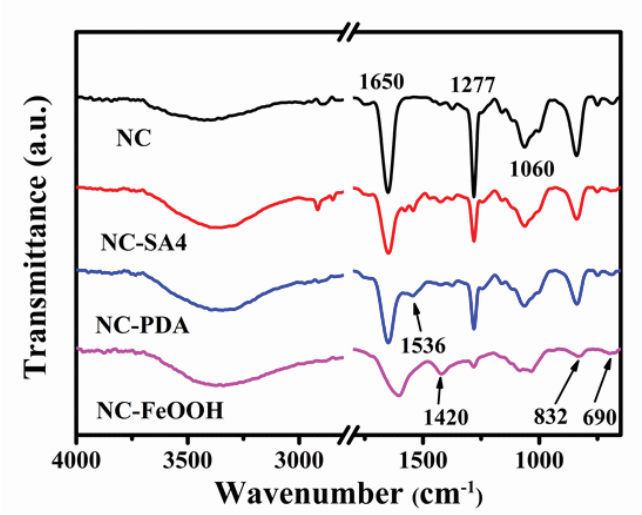

Fig. 2. FTIR spectra of the membranes.

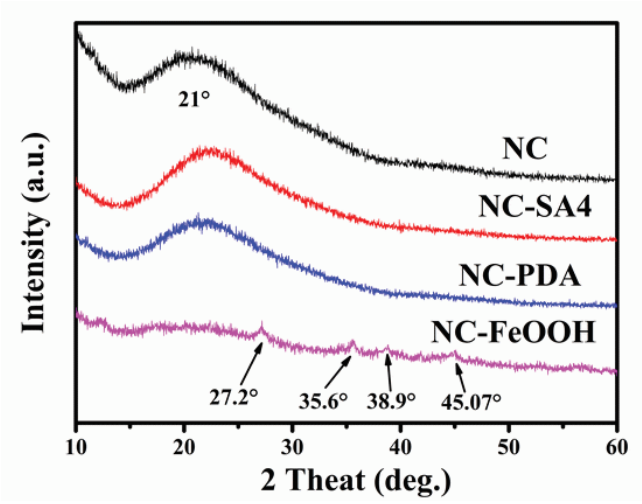

Fig. 3. X-ray diffraction of modified membranes.

amorphous structure and showed only one diffuse diffraction peak at about 21°. After mineralization, diffraction peaks appeared at 27.1° (310), 35.5° (211), 38.8° (301) and 45.1° (411) which were determined by the JCPDS card No. 34-1266 of β-FeOOH indicating the successful deposition of β-FeOOH nanorods on the membrane surface.

3.3. Analysis of membranes surface roughness

The optical profilometry images and average surface roughness (Ra) of the membranes is shown in Fig. 4. The Ra of the NC membrane was about 0.86 μm which meaned the membrane surface was relatively slippery. After the SA layer was deposited on the membranes surface via vacuum filtration, the Ra of the NC-SA membrane slightly increased to about 0.92 μm which could be nearly neglected. When the PDA was coated on the surface of SA layer, the Ra of the NC-PDA membrane slightly increased to about 1.01 μm which mainly due to the aggregation of polydopamine nanoparticles. After the *in suit* mineralization to generate β-FeOOH nanorods, the Ra of the NC-FeOOH membrane was about 1.19 μm primarily owing to the hierarchical structures of nanorods. The above-results indicated that the surface roughness of the films exhibited moderate growth tendency along with the modification.

3.4. Surface wettability of the membranes

The static water contact angle (WCA) was used to characterize the surface wettability of the membranes. As we known, surface hydrophilic modification was an acknowledged method to enhance the antifouling property of the membranes, the formation of tightly bounded water layers on the membranes surface would prevent the adsorption of pollutants via repulsive hydration forces. When the water drop was dropped onto the NC membrane, the WCA was about 55° and reduced to 0° within 60 s which could be assigned to the inherent hydrophilicity. The WCA for the NC-SA4 membrane was about 20° (~3 s) and it gradually declined to 0° within 30 s which illustrated the excellent hydrophilic property of the membrane. Then the PDA was deposited on the surface of the NC-SA4 membrane, the water droplet spread rapidly on the membrane surface within 3 s and the WCA decreased sharply to 0°. Finally the β-FeOOH nanorods was induced to grow on the surface of PDA layer, the membrane still exhibited excellent wettability due to the hydrophilicity and loose nanostructures formed by the nanorods.

3.5. Separation performance for protein solutions

The water flux variation of protein solution and the corresponding flux recovery ratio (FRR%) of the first test are shown in Fig. 6. The filtration tests of pure water and protein solutions (BSA and Lyz) were evaluated by the composite membranes at 0.1 MPa. As we know, the isoelectric point (pI) of BSA and Lyz were about 4.8 and 11 respectively, the pI of PDA was close to 4.0, the pI of β-FeOOH was about 6.5~6.7 in PBS buffer solution (pH 7.0). The water flux curves decreased sharply at the beginning, then gradually became flat during the first round of the filtration as a result of the membrane fouling reached a dynamic equilibrium. Compared with the NC-SA4 membrane, the NC-SA6 membrane possessed a lower permeate flux with thicker barrier layer. The modified side of membranes surface were negatively charged in PBS buffer solution owing to the protonation effect. During the filtration of BSA solution, the composite membranes showed well antifouling property attribute to the electrostatic repulsion effect (Donnan effect) and excellent hydrophilicity, the BSA particles were difficult to adsorb or deposit on the membranes surface. The performance of NC-FeOOH membrane was the optimal among the modified membranes. Except for the above advantages, the nanoarchitecture formed by the β-FeOOH nanorods was another factor which would further weaken the interaction between the pollutants and the membranes. After first cycle filtration, the membranes were simply washed with tap water and the recovery pure water flux was measured, the FRR was about 78.4%, 84.2%, 82.6% and 86.1%, respectively which

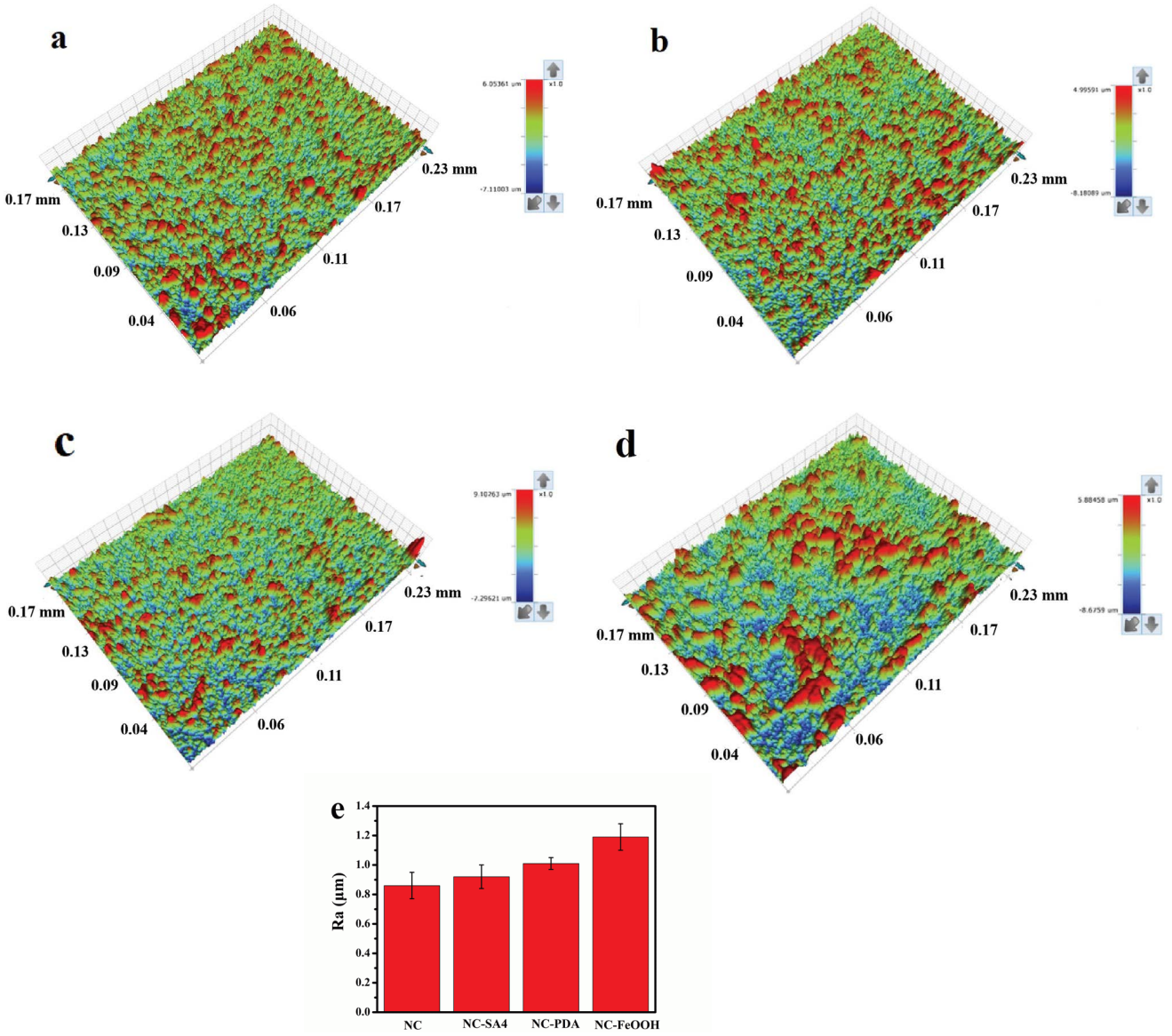

Fig. 4. The optical profilometry images of membranes, (a) NC, (b) NC-SA4, (c) NC-PDA, (d) NC-FeOOH and (e) the corresponding Ra of the membranes.

meaned the increasing BSA resistance functionality. The BSA rejection were about 85.4%, 86.8%, 86.2% and 87.4%, respectively and maintained this level in three cycles of separation. The water flux curves of Lyz solution were similiar with the BSA solution (shown in Fig. 6b), but the antifouling ability expressed worse mainly due to the opposite charges between the Lyz particles and modified sides. The attenuation tendency of the curves exhibited more obvious and the FRR decreased to about 70%, the rejection rate of Lyz particles was in the range of 75%~80%. The Lyz particles with positive charges would adsorbed on the membranes surface more easily via electrostatic interaction causing irreversible fouling. In order to evaluate reusable performance of the membranes, the other two cycles of protein solutions ultrafiltration were carried out and are shown in Fig. 6a and b. The flux of NC-FeOOH membranes remained at about 85% of initial flux after three times of BSA ultrafiltration. The outstanding flux recovery property of the composite membranes ensured the long-run utilization time and operation reliability. The attenuation of water flux curves were more serious during the recycling filtration tests of Lyz solution mainly due to the electrostatic attraction effect. Lyz molecules could exist stably at modified layer, which consequently resulted in an increase of reversible fouling. The results of the protein filtration tests indicated that the combination effect of superhydrophilicity, Donnan effect and nanostructure would effectively promote the antifouling ability of the membranes and ensure the operation reliability.

3.6. Separation performance of oil in water emulsions

The surfactant stabilized oil in water emulsions with a droplet size at the micro- and nanometer scale were

prepared and applied in the separation test. The water flux variation of oil in water emulsions are shown in Fig. 7. It could be seen that the permeate flux decreased sharply in the initial stage, and then reached to a steady state. The appearance of the NC-SA4, NC-SA6 and NC-PDA membranes surface were comparatively uniform and smooth

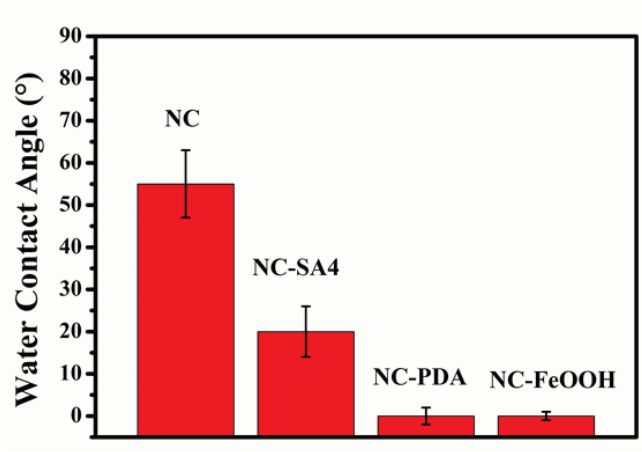

Fig. 5. The static water contact angle of the membranes.

which would cause oil droplets to absorb on the membranes surface more easily comparing with the roughness structure. The antifouling ability mainly depended on the hydrophilicity of the membranes which could form hydration layer with surrounding water molecules to resist oil droplets adsorption. The filtration efficiency of the NC-SA6 membrane was lower compared with the NC-SA4 membrane due to the higher transmembrane pressure. The thickness of SA layer was the crucial factor which the high oil rejection corresponding to low water flux. The permeate flux of the NC-FeOOH membrane remained best among the composite membranes which maybe owing to the combination effect of superwettability and roughness structure. The superhydrophilic and nanoarchitecture could form small voids between the small oil droplets and the nanorods which made the water molecules penetrate through it more easily. After the first cycle, the FRR of the composite membranes were 80.4%, 84.6%, 82.3% and 87.8%, respectively. The oil rejection of the composite membranes were in sequence about 87.5%, 92.4%, 90.3% and 91.8%, and it increased slightly in the following two cycles. The pore size exclusion and superwettability can effectively reduce the contact area between oil droplets and membranes surface. It can be seen that during the three cycles of separation, the flux curves of NC-FeOOH

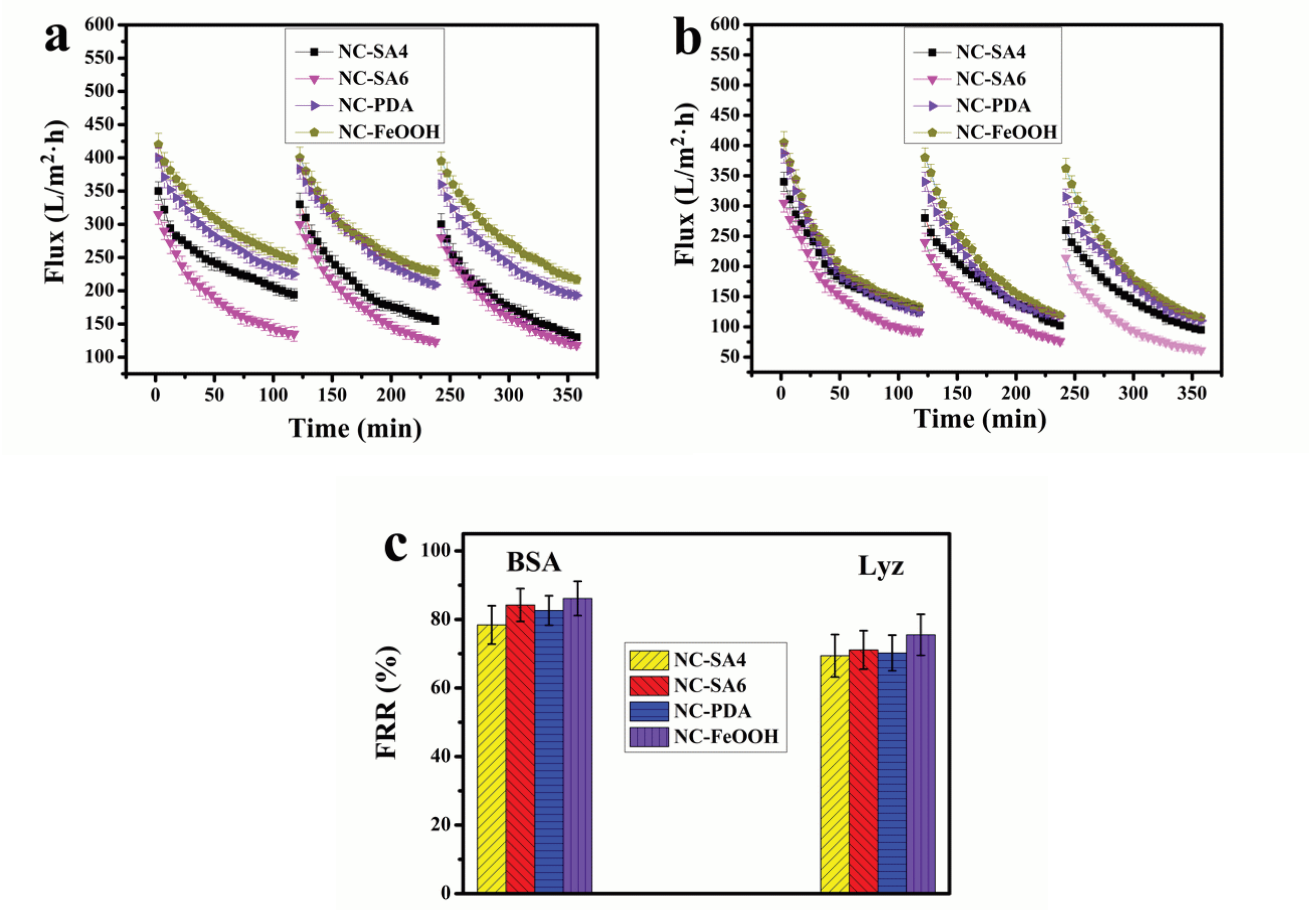

Fig. 6. Flux variation of composite membranes during three cycles of ultrafiltration protein solution (a) BSA, (b) Lyz (pH = 7), and FRR% of the composite membranes during the first round of filtration (c).

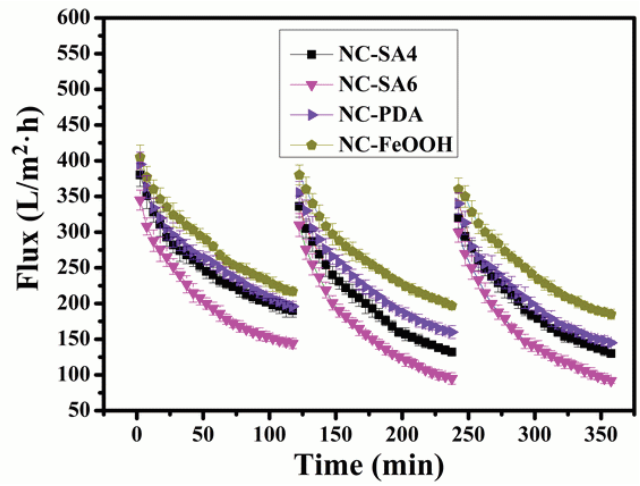

Fig. 7. Performance cycles of membranes when separating oil in water emulsions.

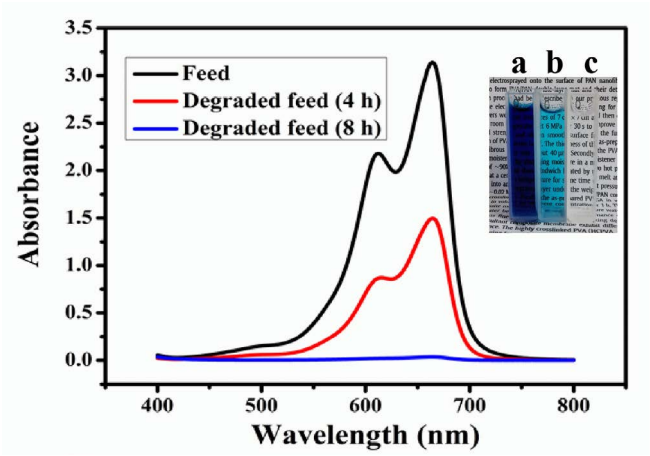

Fig. 8. UV-Vis absorbance and digital photographs, (a) original Methylene blue solution, (b) solution photodegraded 4 h, and (c) solution photodegraded 8 h.

membrane remained at a higher level compared with other composite membranes. Generally speaking, the NC-FeOOH membranes was the optimal selection for the long-term use in oil/water treatment which possessed outstanding flux recovery property and antifouling ability.

3.7. Static self-cleaning property of the membranes

Synthetic dyes were widely used in various fields, while their discharge into environment led to severe environmental problems. Methylene blue was selected as the model sample to explore the photocatalytic performance of the NC-FeOOH membranes under visible light in a transparent container. The dye solution faded lightly after degradation for 4 h, and further became colorless after 8 h. The β-FeOOH nanorods would induce H_2O_2 to generate sufficient hydroxyl radicals according to the photo-Fenton catalytic mechanism. The conjugated chromophore structure of Methylene blue molecules were destroyed and gradually degraded into small organic/inorganic molecules or/and ions matters [36]. The above-result indicated that the NC-FeOOH membranes had not only excellent antifouling performance but also satisfying photo-Fenton catalytic activity. We believed these results would broaden the territory for potential application of the composite membranes in wastewater treatment.

4. Conclusion

In summary, we prepared composite UF membrane with the sodium alginate (SA) as ultrathin hydrophilic barrier layer and nitrocellulose (NC) porous membrane as substrate via vacuum filtration method. Then the PDA was deposited on the surface of SA layer by self-polymerization and β-FeOOH nanorods were induced to grow on PDA layer by bio-mineralization mechanism. The composite membranes showed prominent antifouling ability in the filtration tests of neutral BSA solution mainly due to the membranes superhydrophilicity and electrostatic repulsion effect. The results of separation experiments demonstrated that the NC-FeOOH membrane was the optimum selection owing to the superwettability and hierarchical nanostructure. In addition, the NC-FeOOH membrane possessed photocatalytic antifouling functions and recycling properties which will further benefit its potential application in wastewater treatment. Overall, this research provided a facile and convenient way to prepare a novel composite ultrafiltration membrane with excellent antifouling property and recyclability.

Acknowledgement

The work was supported by Scientific Research Fund of Jiangxi Provincial Education Department (GJJ201816).

References

[1] H.B. Park, B.D. Freeman, Z.-B. Zhang, M. Sankir, J.E. McGrath, Highly chlorine-tolerant polymers for desalination, Angew. Chem. Int. Ed., 47 (2008) 6019–6024.
[2] Z. Chu, Y. Feng, S. Seeger, Oil/water separation with selective superantiwetting/superwetting surface materials, Angew. Chem. Int. Ed., 54 (2015) 2328–2338.
[3] H. Zhang, J. Zheng, Z. Zhao, C.C. Han, Role of wettability in interfacial polymerization based on PVDF electrospun nanofibrous scaffolds, J. Membr. Sci., 442 (2013) 124–130.
[4] S. Mostafa Mokhtari, A. Rahimpour, A.A. Shamsabadi, S. Habibzadeh, M. Soroush, Enhancing performance and surface antifouling properties of polysulfone ultrafiltration membranes with salicylate-alumoxane nanoparticles, Appl. Surf. Sci., 393 (2017) 93–102.
[5] N.A.B.M. Salleh, A.M. Afifi, F.B. Mohamed Zuki, N. Muhamad Sarih, K. Kalantari, E. Niza Mohamad, Studies on properties and adsorption ability of bilayer chitosan/PVA/PVDF electrospun nanofibrous, Desal. Water Treat., 206 (2020) 177–188.
[6] G. Kwon, E. Post, A. Tuteja, Membranes with selective wettability for the separation of oil–water mixtures, MRS Commun., 5 (2015) 475–494.
[7] Z. Pan, S. Cao, J. Li, Z. Du, F. Cheng, Anti-fouling TiO_2 nanowires membrane for oil/water separation: synergetic effects of wettability and pore size, J. Membr. Sci., 572 (2019) 596–606.
[8] Z. Zhao, J. Zheng, M. Wang, H. Zhang, C.C. Han, High performance ultrafiltration membrane based on modified chitosan coating and electrospun nanofibrous PVDF scaffolds, J. Membr. Sci., 394 (2012) 209–217.

[9] Y.-F. Yang, L.-S. Wan, Z.-K. Xu, Surface engineering of microporous polypropylene membrane for antifouling: a mini-review, J. Adhes. Sci. Technol., 25 (2011) 245–260.
[10] A.V. Bildyukevich, T.V. Plisko, A.A. Shustikov, Yu. S. Dzyazko, L.M. Rozhdestvenska, S.A. Pratsenko, Effect of the solvent nature on the structure and performance of poly(amide-imide) ultrafiltration membranes, J. Mater. Sci., 55 (2020) 9638–9654.
[11] N. Helali, M. Rastgar, M.F. Ismail, M. Sadrzadeh, Development of underwater superoleophobic polyamide-imide (PAI) microfiltration membranes for oil/water emulsion separation, Sep. Purif. Technol., 238 (2019) 116451, doi: 10.1016/j.seppur.2019.116451.
[12] L.-J. Zhu, L.-P. Zhu, J.-H. Jiang, Z. Yi, Y.-F. Zhao, B.-K. Zhu, Y.-Y. Xu, Hydrophilic and anti-fouling polyethersulfone ultrafiltration membranes with poly(2-hydroxyethyl methacrylate) grafted silica nanoparticles as additive, J. Membr. Sci., 451 (2014) 157–168.
[13] A. Xie, J. Cui, J. Yang, Y. Chen, J. Dai, J. Lang, C. Li, Y. Yan, Photo-Fenton self-cleaning membranes with robust flux recovery for an efficient oil/water emulsion separation, J. Mater. Chem. A, 7 (2019) 8491–8502.
[14] M. Wang, Z. Xu, Y. Hou, P. Li, H. Sun, Q. Jason Niu, Photo-Fenton assisted self-cleaning hybrid ultrafiltration membranes with high-efficient flux recovery for wastewater remediation, Sep. Purif. Technol., 249 (2020) 117159, doi: 10.1016/j.seppur.2020.117159.
[15] Q. Wu, N. Chen, L. Li, Q. Wang, Structure evolution of melt-spun poly(vinyl alcohol) fibers during hot-drawing, J. Appl. Polym. Sci., 124 (2012) 421–428.
[16] T.A. Misev, R. van der Linde, Powder coatings technology: new developments at the turn of the century, Prog. Org. Coat., 34 (1998) 160–168.
[17] G. Zhang, P. Wang, X. Zhang, C. Xiang, L. Li, Preparation of hierarchically structured PCL superhydrophobic membrane via alternate electrospinning/electrospraying techniques, J. Polym. Sci. Pol. Phys., 57 (2019) 421–430.
[18] G. Song, J. Li, J. Yu, Y. Wang, J. Zhu, Z. Hu, Preparation and characterization of PES-C/PVPP nanofibrous composite membranes via soultion-blowing, IOP Conf. Ser.: Earth Environ. Sci., 186 (2018) 012029, doi: 10.1088/1755-1315/186/2/012029.
[19] Z. Shi, W. Zhang, F. Zhang, X. Liu, D. Wang, J. Jin, L. Jiang, Ultrafast separation of emulsified oil/water mixtures by ultrathin free-standing single-walled carbon nanotube network films, Adv. Mater., 25 (2013) 2422–2427.
[20] L. Hu, S. Gao, Y. Zhu, F. Zhang, L. Jiang, J. Jin, An ultrathin bilayer membrane with asymmetric wettability for pressure responsive oil/water emulsion separation, J. Mater. Chem. A, 3 (2015) 23477–23482.
[21] Y. Jiang, J. Hou, J. Xu, B. Shan, Switchable oil/water separation with efficient and robust Janus nanofiber membranes, Carbon, 115 (2017) 477–485.
[22] C. Xu, Y. Xu, J. Zhu, Photocatalytic antifouling graphene oxide-mediated hierarchical filtration membranes with potential applications on water purification, ACS Appl. Mater. Interfaces, 6 (2014) 16117–16123.
[23] Q. Zhang, G. Rao, J. Rogers, C. Zhao, L. Liu, Y. Li, Novel anti-fouling Fe_2O_3/TiO_2 nanowire membranes for humic acid removal from water, Chem. Eng. J., 271 (2015) 180–187.
[24] C. Wang, F. Yang, F. Meng, H. Zhang, Y. Xue, G. Fu, High flux and antifouling filtration membrane based on non-woven fabric with chitosan coating for membrane bioreactors, Bioresour. Technol., 101 (2010) 5469–5474.
[25] R. Chang, S. Ma, X. Guo, J. Xu, C. Zhong, R. Huang, J. Ma, Hierarchically assembled graphene oxide composite membrane with self-healing and high-efficiency water purification performance, ACS Appl. Mater. Interfaces, 11 (2019) 22324–22333.
[26] S. Khakpour, Y. Jafarzadeh, R. Yegani, Incorporation of graphene oxide/nanodiamond nanocomposite into PVC ultrafiltration membranes, Chem. Eng. Res. Des., 152 (2019) 60–70.
[27] F.A.A. Ali, J. Alam, A.K. Shukla, M. Alhoshan, J.M. Khaled, W.A. Al-Masry, N.S. Alharbi, M. Alam, Graphene oxide-silver nanosheet-incorporated polyamide thin-film composite membranes for antifouling and antibacterial action against *Escherichia coli* and bovine serum albumin, J. Ind. Eng. Chem., 80 (2019) 227–238.
[28] S. Zarghami, T. Mohammadi, M. Sadrzadeh, B. Van der Bruggen, Bio-inspired anchoring of amino-functionalized multi-wall carbon nanotubes (N-MWCNTs) onto PES membrane using polydopamine for oily wastewater treatment, Sci. Total Environ., 711 (2020) 134951, doi: 10.1016/j.scitotenv.2019.134951.
[29] S. Mona Mirmousaei, M. Peyravi, M. Khajouei, M. Jahanshahi, S. Khalili, Preparation and characterization of nano-filtration and its photocatalytic abilities via pre-coated and self-forming dynamic membranes developed by ZnO, PAC and chitosan, Water Sci. Technol., 80 (2019) 2273–2283.
[30] M. Wang, Z. Xu, Y. Guo, Y. Hou, P. Li, Q. Jason Niu, Engineering a superwettable polyolefin membrane for highly efficient oil/water separation with excellent self-cleaning and photocatalysis degradation property, J. Membr. Sci., 611 (2020) 118409, doi: 10.1016/j.memsci.2020.118409.
[31] X. Zhao, L. Cheng, N. Jia, R. Wang, L. Liu, C. Gao, Polyphenol-metal manipulated nanohybridization of CNT membranes with FeOOH nanorods for high-flux, antifouling and self-cleaning oil/water separation, J. Membr. Sci., 600 (2020) 117857, doi: 10.1016/j.memsci.2020.117857.
[32] Y. Lv, C. Zhang, A. He, S.-J. Yang, G.-P. Wu, S.B. Darling, Z.-K. Xu, Photocatalytic nanofiltration membranes with self-cleaning property for wastewater treatment, Adv. Funct. Mater., 27 (2017) 1700251, doi: 10.1002/adfm.201700251.
[33] G. Song, K. Luo, J. Yu, Y. Wang, J. Zhu, Z. Hu, High performance ultrafiltration composite membranes based on nanofibrous substrate with PDA coating and TAPS-NA immobilization, Polym. Plast. Technol. Mater., 58 (2019) 1–14.
[34] X. Li, H. Shan, M. Cao, B. Li, Mussel-inspired modification of PTFE membranes in a miscible THF-Tris buffer mixture for oil-in-water emulsions separation, J. Membr. Sci., 555 (2018) 237–249.
[35] J. Wang, L. Hou, K. Yan, L. Zhang, Q.J. Yu, Polydopamine nanocluster decorated electrospun nanofibrous membrane for separation of oil/water emulsions, J. Membr. Sci., 547 (2018) 156–162.
[36] L. Zhang, Y. He, L. Ma, J. Chen, Y. Fan, S. Zhang, H. Shi, Z. Li, P. Luo, Hierarchically stabilized PAN/β-FeOOH nanofibrous membrane for efficient water purification with excellent antifouling performance and robust solvent resistance, ACS Appl. Mater. Interfaces, 11 (2019) 34487–34496.